A Stochastic Optimization Framework for the Coordinated Operation of Renewable–Computational Energy Bases

1st Yaxuan Zhu
Beijing Normal University Affiliated Experimental High School
Beijing, China
zoe507.zhu@gmail.com

***Abstract*—This paper proposes a stochastic optimization framework for the coordinated operation of renewable–computational energy bases, where large-scale wind–solar generation is jointly scheduled with flexible computing workloads. To capture uncertainties in renewable output and electricity prices, intraday scenarios are generated using an autoregressive random process, while computational demand uncertainty is represented through independent temporal perturbations. The model characterizes three classes of computing tasks—PB, AB, and RT—each with distinct delay tolerance, and formulates their cumulative demand, completion dynamics, and waiting-time penalties. A two-stage structure is established in which day-ahead decisions on interconnector exchange are optimized in the master MILP, and intraday operational responses are solved in nonlinear subproblems via generalized Benders decomposition. Case studies show that flexible scheduling of computational tasks effectively alleviates the temporal mismatch between renewable supply and electricity demand, enabling higher consumption of renewable energy and reducing curtailment. The results also reveal that enhancing storage and transmission capacities simultaneously lowers both task delay violations and renewable curtailment, while sole expansion of renewable installed capacity increases balancing pressure. Overall, the proposed framework demonstrates the significant potential of computation–energy synergy for improving the reliability and efficiency of future high-renewable power systems.**

***Index Terms*—Renewable–computational energy base; stochastic optimization; flexible computing load; generalized Benders decomposition**

I. Introduction

With the rapid expansion of wind and photovoltaic (PV) generation capacity, the power system structure is gradually shifting from a controllable fossil-fuel-dominated system to a stochastic, renewable-dominated one. This structural transition significantly reduces the controllability of power supply, while output volatility and uncertainty continue to increase, posing severe challenges to the traditional paradigm of balancing supply and demand using conventional generators. In this context, maintaining system energy balance and operational stability under high renewable penetration has become one of the core research issues in modern power systems [1]. Moreover, the planning and expansion of renewable generation systems must also account for carbon emission constraints, which influence generation layout and capacity decisions [2].

Existing balancing measures primarily include energy storage systems and inter-regional transmission lines. Energy storage can smooth power fluctuations across time scales, while transmission lines provide spatial compensation through inter-area exchanges. However, both solutions are constrained by capacity, efficiency, and economic considerations, making it challenging to rely solely on these resources to support the flexible operation of high-renewable systems. Consequently, the adjustable potential of demand-side resources has increasingly become a critical supplement to system flexibility [3].

In recent years, driven by the rapid development of the digital economy, data centers have emerged as representative high-power-demand loads. The computational tasks they host exhibit inherent flexibility in both temporal and spatial dimensions [4]. Computational workloads can be categorized into three types based on business characteristics: periodic batch (PB) tasks, aperiodic batch (AB) tasks, and real-time (RT) tasks. The first two types possess a degree of scheduling flexibility, allowing time-shifting or execution adjustments to participate in system-level regulation, thereby providing multi-layered flexible demand resources for the power system. This offers a novel approach to achieving dynamic supply-demand matching in scenarios where supply-side flexibility is limited.

Building on this, the present study investigates the participation of computational loads in power system flexibility and develops an optimization framework for the coordinated operation of renewable-energy and computational-load bases. The model simultaneously considers multi-source uncertainties, including renewable generation, electricity prices, and computational demand. By incorporating waiting-time constraints and penalty mechanisms for computational tasks, the framework characterizes their flexible dispatch potential, balancing computational service quality and overall system operational costs. To address the inherent uncertainty and computational complexity, a scenario-based stochastic optimization approach combined with decomposition techniques is employed, enhancing solution efficiency and decision reliability.

To validate the effectiveness and flexibility of the proposed framework, a case study is conducted on a computational–renewable hybrid base integrating wind, PV, and energy storage. Analysis of coordinated supply-demand scheduling results demonstrates that flexible dispatch of computational

979-8-3315-8138-1

loads plays a significant role in mitigating renewable output fluctuations, balancing system power, and improving the utilization efficiency of renewable energy.

II. Modeling of Flexible Computing Loads

On the power supply side, renewable energy sources (RES) such as wind and PV generation exhibit significant randomness and uncontrollability, making their outputs difficult to adjust in accordance with system demand. Although energy storage systems can help balance energy across temporal scales and tie-lines can facilitate power exchange across regions, their effectiveness remains constrained by storage capacity and transmission limits. Consequently, these mechanisms alone are insufficient to ensure the flexible operation of a high-RES system.

Meanwhile, computing loads—emerging as a new category of high energy–consuming demand—often possess inherent flexibility in their operational characteristics. Fully exploiting their temporal or spatial adjustability can help achieve dynamic supply–demand matching when supply-side flexibility is limited, thereby promoting renewable energy accommodation and enhancing system stability.

Fig. 1 demonstrates how supply-side and demand-side adjustments jointly contribute to real-time balancing. The original renewable generation and computing load profiles exhibit a clear mismatch. By activating both supply-side measures and demand-side measures, the system is able to reshape both curves, achieving an alignment between supply and demand that would not be attainable through supply-side flexibility alone.

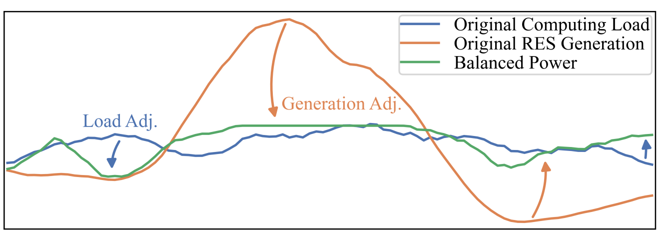

Fig. 1. Illustration of coordinated power balancing enabled by adjustments on both the supply side.

Computing tasks in data centers are typically classified into three categories: PB tasks, AB tasks, and RT tasks. These categories differ substantially in terms of their arrival patterns, delay sensitivity, and stochasticity.

1) Periodic Batch (PB) Tasks

PB tasks are submitted repetitively at fixed intervals according to predefined business logic [5], such as daily scheduled data analytics. In the day-ahead stage, their workload demand is deterministic and exhibits minimal intra-day fluctuation, making them suitable as controllable and schedulable flexible computing loads.

2) Aperiodic Batch (AB) Tasks

AB tasks are triggered randomly by users, with stochastic submission times and computational requirements [6]. Although their randomness is weaker than that of RT tasks, they still exhibit certain intra-day uncertainties [7]. Due to their higher tolerance for execution delay, AB tasks can be shifted to periods of lower system load to absorb renewable power fluctuations.

3) Real-Time (RT) Tasks

RT tasks demand immediate response and include applications such as financial transactions, disaster warning systems, and high-definition video communication [8]. These tasks exhibit the highest degree of randomness in arrival times, resource requirements, and concurrency, and must be executed without delay, thus having the highest scheduling priority.

In the modeling framework, both computing demand and supply are represented using continuous variables. For any task category $x \in X = \{\mathrm{PB}, \mathrm{AB}, \mathrm{RT}\}$, the computing demand is defined as $D^x_{s,t}$, and the computing capacity allocated by the data center is defined as $u^x_{s,t}$, where $t \in \mathcal{T} = \{1, 2, ..., T\}$ denotes the time index, and $s \in \mathcal{S} = \{1, 2, ..., S\}$ denotes the scenario index.

The introduction of scenario indices enables the explicit representation of multi-source uncertainties within the optimization framework. In addition to the stochastic nature of computing tasks, uncertainties on the power supply side—such as wind and PV generation outputs and day-ahead electricity prices—must also be considered. To capture these uncertainties, a scenario sampling approach is adopted to construct the scenario set $\mathcal{S}$, which characterizes the possible realizations of uncertain parameters across future periods.

III. Optimization Model

A. Objective Function

The objective function consists of two components: (i) the economic cost (or revenue) associated with electricity purchase and sale through the tie-line, denoted as C_{T}, and (ii) the penalty cost arising from excessive waiting time of computing tasks, denoted as C_{W}.

B. Computing Task Model

For any task category $x \in X$, the computing load is characterized by the cumulative demand $R^x_{s,t}$, cumulative completion $C^x_{s,t}$, waiting demand $w^x_{s,t}$, and delay time $T^x_{s,t}$. For any $s \in \mathcal{S}$ and $t \in \mathcal{T}$, we have:

$$\begin{aligned} R^x_{s,t} &= \sum_{\tau=1}^{t} D^x_{s,\tau}, \quad C^x_{s,t} = \sum_{\tau=1}^{t} u^x_{s,\tau}, \\ w^x_{s,t} &= R^x_{s,t} - C^x_{s,t}, \\ T^x_{s,t} &= \min_{\tau \geq t} \{\tau - t \mid C^x_{s,\tau} \geq R^x_{s,t}\} \end{aligned} \tag{1}$$

The penalty cost due to excessive waiting time is expressed as:

$$C_{\mathrm{W}} = \sum_{x \in X} \sum_{s \in \mathcal{S}, t \in \mathcal{T}} \xi_s \left(\lambda^x \max\{T^x_{s,t} - \Delta^x, 0\} \right) \tag{2}$$

where Δ^x denotes the maximum allowable waiting time for task category x, with $\Delta^{\mathrm{RT}} = 0$, and λ^x is the penalty coefficient for category x , and ξ_s is the probability weight of scenario s.

979-8-3315-8138-1

The constraints related to computing tasks include:

1) Non-negativity of waiting demand

$$w_{s,t}^{x} \geq 0, \quad x \in X, s \in \mathcal{S}, t \in \mathcal{T} \tag{3}$$

2) Cross-day upper bound and periodicity

$$w_{s,T}^{x} \leq \Gamma^{x}, \quad w_{s,1}^{x} = w_{s,T+1}^{x}, \quad x \in X \; s \in \mathcal{S} \tag{4}$$

where Γ^{x} represents the maximum allowable carry-over workload for category x.

3) Power consumption of the computing center The power demand of the computing center is linked to the allocated computing capacity by:

$$P_{s,t} = P_{\mathrm{idle}} + (P_{\mathrm{peak}} - P_{\mathrm{idle}})u_{s,t}, \quad s \in \mathcal{S}, t \in \mathcal{T} \tag{5}$$

C. Power Supply Model

1) Wind and PV generation limits

Decision variables include the wind power outputs $P_{\mathrm{W},s,t}$ and the PV power outputs $P_{\mathrm{P},s,t}$, both defined over $\mathcal{S} \times \mathcal{T}$:

$$\begin{aligned} 0 \leq P_{\mathrm{W},s,t} \leq \rho_{\mathrm{W},s,t} S_{\mathrm{W}}, \quad s \in \mathcal{S},\ t \in \mathcal{T} \\ 0 \leq P_{\mathrm{P},s,t} \leq \rho_{\mathrm{P},s,t} S_{\mathrm{P}}, \quad s \in \mathcal{S},\ t \in \mathcal{T} \end{aligned} \tag{6}$$

where $\rho_{\mathrm{W},s,t}$ and $\rho_{\mathrm{P},s,t}$ are wind and PV availability factors under scenario s and time t, and S_{W} and S_{P} are installed capacities of wind and PV plants.

2) Tie-line modeling

Day-ahead tie-line decision variables include $P_{\mathrm{T},t}^{\mathrm{DA}}$, $P_{\mathrm{T},t}^{\mathrm{DA,b}}$, $P_{\mathrm{T},t}^{\mathrm{DA,s}}$, all defined over $\mathcal{T}$:

$$\begin{aligned} P_{\mathrm{T},t}^{\mathrm{DA}} = P_{\mathrm{T},t}^{\mathrm{DA,b}} - P_{\mathrm{T},t}^{\mathrm{DA,s}} \\ 0 \leq P_{\mathrm{T},t}^{\mathrm{DA,b}} \leq S_{\mathrm{T}}, \quad 0 \leq P_{\mathrm{T},t}^{\mathrm{DA,s}} \leq S_{\mathrm{T}} \end{aligned} \tag{7}$$

Intra-day tie-line decision variables include $P_{\mathrm{T},s,t}^{\mathrm{ID}}$, $P_{\mathrm{T},s,t}^{\mathrm{ID,b}}$, $P_{\mathrm{T},s,t}^{\mathrm{ID,s}}$, all defined over $\mathcal{S} \times \mathcal{T}$:

$$\begin{aligned} P_{\mathrm{T},s,t} = P_{\mathrm{T},t}^{\mathrm{DA}} + P_{\mathrm{T},s,t}^{\mathrm{ID}} \\ P_{\mathrm{T},s,t}^{\mathrm{ID}} = P_{\mathrm{T},s,t}^{\mathrm{ID,b}} - P_{\mathrm{T},s,t}^{\mathrm{ID,s}} \\ 0 \leq P_{\mathrm{T},s,t}^{\mathrm{ID,b}} \leq S_{\mathrm{T}} - P_{\mathrm{T},t}^{\mathrm{DA}}, \quad 0 \leq P_{\mathrm{T},s,t}^{\mathrm{ID,s}} \leq S_{\mathrm{T}} + P_{\mathrm{T},t}^{\mathrm{DA}} \end{aligned} \tag{8}$$

In (7) and (8), the superscripts "DA" and "ID" denote the day-ahead and intra-day stages, respectively, while the superscripts "b" and "s" represent buying and selling, respectively.

3) Energy storage model

Storage-related decision variables include the net storage power $P_{\mathrm{S},s,t}$, the discharging power $P_{\mathrm{S},s,t}^{\mathrm{dis}}$, the charging power $P_{\mathrm{S},s,t}^{\mathrm{ch}}$ and the state of charge (SOC) $E_{\mathrm{S},s,t}$:

$$\begin{aligned} P_{\mathrm{S},s,t} = P_{\mathrm{S},s,t}^{\mathrm{dis}} - P_{\mathrm{S},s,t}^{\mathrm{ch}} \\ 0 \leq P_{\mathrm{S},s,t}^{\mathrm{ch}} \leq S_{\mathrm{S,p}}, \quad 0 \leq P_{\mathrm{S},s,t}^{\mathrm{dis}} \leq S_{\mathrm{S,p}} \end{aligned} \tag{9}$$

where $S_{\mathrm{S,p}}$ is the rated charging/discharging power of the storage system.

$$E_{\mathrm{S},s,t} = E_{\mathrm{S},s,t-1} + \eta^{\mathrm{ch}} P_{\mathrm{S},s,t}^{\mathrm{ch}} - P_{\mathrm{S},s,t}^{\mathrm{dis}} / \eta^{\mathrm{dis}} \tag{10}$$

where η^{ch} and η^{dis} denote charging and discharging efficiencies.

4) Power balance

$$P_{s,t} = P_{\mathrm{W},s,t} + P_{\mathrm{P},s,t} + P_{\mathrm{T},s,t} + P_{\mathrm{S},s,t}, s \in \mathcal{S}, t \in \mathcal{T} \tag{11}$$

5) Tie-line economic cost

$$\begin{aligned} C_{\mathrm{T}} = \sum_{t \in \mathcal{T}} \left(\pi_{t}^{\mathrm{DA,b}} P_{\mathrm{T},t}^{\mathrm{DA,b}} - \pi_{t}^{\mathrm{DA,s}} P_{\mathrm{T},t}^{\mathrm{DA,s}} \right) \\ + \sum_{s \in \mathcal{S}, t \in \mathcal{T}} \xi_{s} \left(\pi_{s,t}^{\mathrm{ID,b}} P_{\mathrm{T},s,t}^{\mathrm{ID,b}} - \pi_{s,t}^{\mathrm{ID,s}} P_{\mathrm{T},s,t}^{\mathrm{ID,s}} \right) \end{aligned} \tag{12}$$

where $\pi_{t}^{\mathrm{DA,b}}$, $\pi_{t}^{\mathrm{DA,s}}$, $\pi_{s,t}^{\mathrm{ID,b}}$ and $\pi_{s,t}^{\mathrm{ID,s}}$ are the day-ahead (DA) electricity buying and selling price, and the intraday (ID) electricity buying and selling price at time t, respectively, and ξ_{s} is the probability weight of scenario s.

IV. Solution Approach for the Optimization Model

Before solving the proposed model, it is necessary to stochastically generate possible intraday trajectories for the next day based on the day-ahead forecasts. Considering that the intraday deviations of electricity prices, wind power, and PV output exhibit strong temporal correlation and stationarity, this study adopts a scenario generation method based on a first-order autoregressive process (AR(1)). The temporally correlated random sequence is generated as:

$$\varepsilon_{t} = \phi\, \varepsilon_{t-1} + \sigma\, \xi_{t}, \quad \xi_{t} \sim \mathcal{N}(0,1), \varepsilon_{0} \sim \mathcal{N}\left(0, \frac{\sigma^{2}}{1-\phi^{2}}\right) \tag{13}$$

where $\phi \in (0,1)$ is the autoregressive coefficient controlling temporal dependence, and σ denotes the intensity of random disturbances.

For the computational load demand, whose temporal correlation is relatively weak, independent random disturbances are generated at each time period to construct its intraday deviations. By superimposing or multiplying the generated random sequences onto the day-ahead forecasts, a set of candidate intraday scenarios for the next day can be obtained.

Regarding the solution of the optimization model, a generalized Benders decomposition (GBD) approach [9] is employed. The day-ahead optimization problem is decomposed into a MILP master problem and an NLP subproblem, which are solved iteratively.

V. Case Studies

In this case study, the peak electric load is set as $P_{\mathrm{peak}} =$ 1 p.u., and the maximum computational supply capacity of the data center is also set to 1 p.u. The system parameters are listed in Table I.

TABLE I
System Parameters

P_{peak}	1	P_{idle}	0.25
S_{W}	1.5	S_{P}	3
$S_{\mathrm{S,p}}$	0.25	S_{T}	0.5

A typical day-ahead forecast and the intraday scenarios generated based on the forecast are shown in Fig. 2. In each

979-8-3315-8138-1

subplot, the dark curve represents the day-ahead forecast, while the light and lighter shaded areas indicate the 25%–75% and 5%–95% quantile ranges of the generated scenarios, respectively. As observed from the upper-left subplot, a significant mismatch exists between intraday electricity supply and demand, implying that flexibility from both the supply and demand sides is required for balancing. On the computational side, different types of loads exhibit markedly different levels of randomness: RT loads show the strongest intraday fluctuations, while PB loads exhibit nearly no stochastic variation.

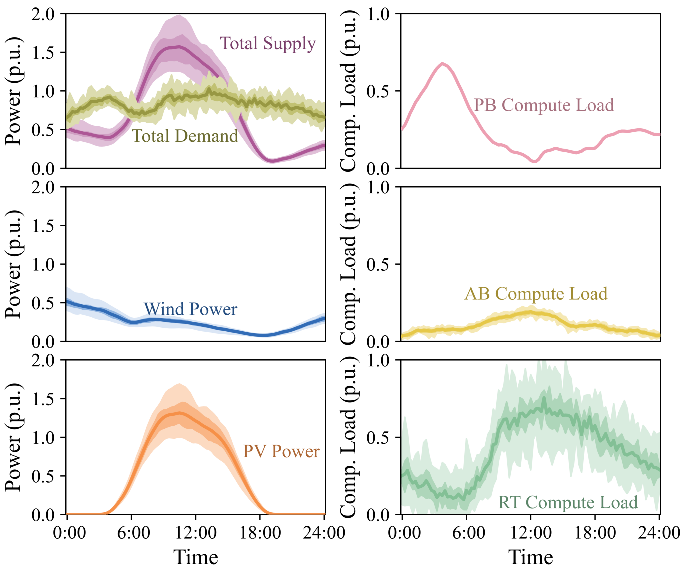

Fig. 2. Day-ahead forecasts and generated intraday scenarios for a typical day.

A typical intraday scenario of the system power balance is illustrated in Fig. 3, and the computational load supply and delay characteristics are shown in Fig. 4. System balance is jointly maintained by flexible adjustments from both supply and demand sides. As observed from Fig. 3, the supply-side balancing relies on wind and PV generation, the energy storage system, and power exchanges via intraday (ID) and day-ahead (DA) interconnectors. During midday, renewable generation significantly exceeds local demand, and part of the surplus is absorbed through storage charging or exported via interconnectors, although some curtailment remains inevitable. In contrast, during the evening when renewable output is insufficient, the system relies on storage discharge and external purchases to compensate.

On the demand side, Fig. 4 demonstrates the adjustment behaviors. From the upper subplot, a clear temporal mismatch can be observed between the renewable supply and the original electric demand—excess supply occurs at noon while deficits appear during night and early morning. Besides supply-side measures, PB and AB loads participate in balancing through task postponement and execution rescheduling, further mitigating supply–demand imbalances. RT loads, due to strict latency constraints, contribute minimally to demand-side flexibility.

Overall, the flexible scheduling of computational loads plays a crucial role in smoothing power fluctuations, enhancing renewable energy utilization, and improving overall system operational efficiency.

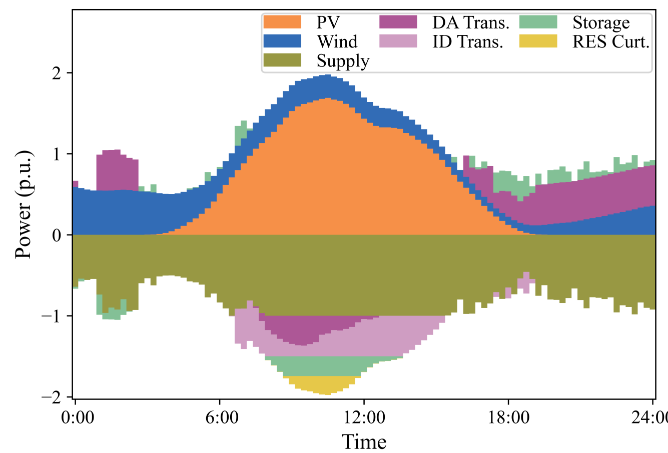

Fig. 3. Power balance of a typical intraday scenario.

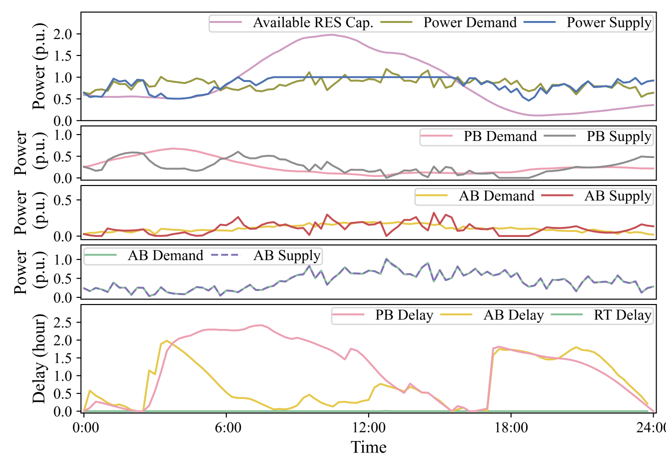

Fig. 4. Computational load demand, supply, and delay response in a typical scenario.

To analyze long-term performance, 200 typical days are selected, each with 100 intraday scenarios. Statistical results are summarized in Fig. 5 and Fig. 6. Fig. 5 presents the delay distributions of the three computational load types, together with the probability and average magnitude of delay violations beyond their maximum allowable thresholds. Although overtime events occur under extreme scenarios, both their probability and average duration remain low. Fig. 6 shows the daily available renewable energy, actual renewable generation, and curtailed energy. Significant variability is observed in daily generation, and the surplus or deficit energy is balanced through the interconnector.

Table II presents the sensitivity results of the delay violation rates of the three computational load types (η^{PB}, η^{AB}, η^{RT}) and renewable curtailment (E_{curt}) with respect to the

979-8-3315-8138-1

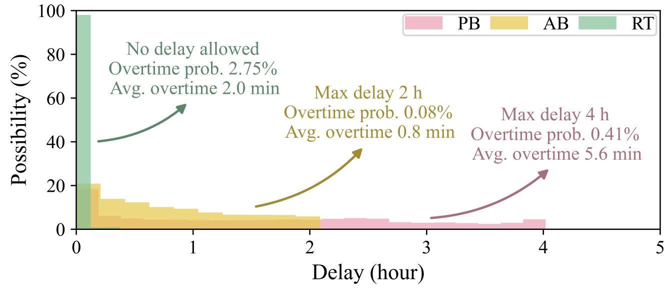

Fig. 5. Statistical delay distributions of PB, AB, and RT computational loads.

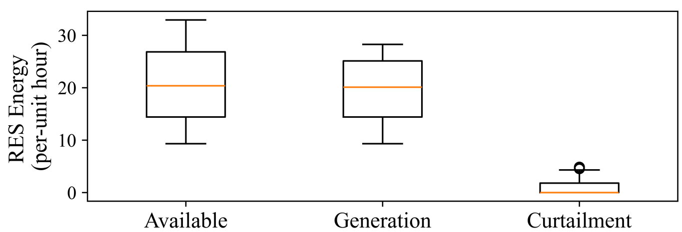

Fig. 6. Daily renewable availability, generation, and curtailment.

main system capacity parameters. The results show that the delay violation rates of the three load types exhibit negative sensitivity to wind, PV, storage, and interconnector capacities. This indicates that enhanced supply-side capability reduces the probability of delay violations, with PB loads being the most sensitive, followed by AB loads, while RT loads remain largely unaffected.

In contrast, renewable curtailment exhibits mixed sensitivities: positive with respect to wind and PV capacities, implying that larger renewable installations introduce higher surplus energy; and negative with respect to storage and interconnector capacities, indicating that enhanced flexibility mitigates curtailment. Overall, increasing supply-side flexibility (storage and interconnection) reduces both computational delay risks and renewable curtailment, whereas simply expanding renewable capacity may increase system balancing pressure.

VI. Conclusion

In this study, a coordinated scheduling framework integrating renewable generation, energy storage, interconnector exchange, and flexible computation loads was proposed to enhance supply–demand balancing in renewable-rich power systems. By modeling the distinct temporal characteristics and flexibility levels of PB, AB, and RT computational tasks, the framework effectively exploits the inherent adjustability of data center workloads to complement the limited flexibility on the supply side. Case studies based on large sets of day-ahead forecasts and intraday scenarios demonstrate that flexible scheduling of computational loads significantly mitigates the temporal mismatch between renewable generation and electricity demand, thereby reducing renewable curtailment and improving overall system efficiency. Sensitivity analysis further reveals that enhancing supply-side flexibility—through increased storage or transmission capacity—jointly reduces both task delay violations and renewable curtailment, whereas simply scaling up renewable installations may intensify system balancing challenges. Overall, the results highlight the promising role of computation–energy synergy in supporting reliable and efficient operation of future high-renewable power systems. Future work may extend the proposed framework by incorporating more advanced dispatch and control techniques, such as adaptive or learning-based strategies, to further enhance the utilization of existing infrastructure under increased uncertainty.

TABLE II
Sensitivity of Delay Violation Rates and Renewable Curtailment to Capacity Parameters

	η^{PB} (%)	η^{AB} (%)	η^{RT} (%)	E_{curt} (p.u. h)
S_{W} (p.u.)	-5.699	-3.007	-0.003	1.787
S_{P} (p.u.)	-1.157	-0.843	-0.001	3.923
$S_{\mathrm{S,p}}$ (p.u.)	-1.739	-0.835	-0.001	-3.126
S_{T} (p.u.)	-2.652	-1.363	-0.001	-5.716

References

[1] Y. Ye et al., “Harvesting spatial-temporal load migration flexibility of data centers: A chance-constrained bi-level optimization model with endogenously formed risk-reflective locational prices,” Applied Energy, vol. 402, p. 126971, Jan. 2026, doi: 10.1016/j.apenergy.2025.126971

[2] W. Liao, D. Liu, Y. Xue, Y. Wu, F. Xue, and K. Chang, “Power generation expansion planning considering natural disaster scenarios under carbon emission trajectory constraints,” Appl. Energy, vol. 361, p. 122832, May 2024, doi: 10.1016/j.apenergy.2024.122832.

[3] A. Nikoobakht, J. Aghaei, M. Shafie-Khah, and J. P. S. Catalao, “Assessing Increased Flexibility of Energy Storage and Demand Response to Accommodate a High Penetration of Renewable Energy Sources,” IEEE Trans. Sustain. Energy, vol. 10, no. 2, pp. 659–669, Apr. 2019, doi: 10.1109/TSTE.2018.2843161..

[4] Y. Wang, Q. Guo, and M. Chen, “Providing load flexibility by reshaping power profiles of large language model workloads,” Adv. Appl. Energy, vol. 19, p. 100232, Sep. 2025, doi: 10.1016/j.adapen.2025.100232.

[5] Y. Cao et al., “Data-driven flexibility assessment for internet data center towards periodic batch workloads,” Appl. Energy, vol. 324, p. 119665, Oct. 2022, doi: 10.1016/j.apenergy.2022.119665.

[6] C. Wang, Y. Bai, and D. Sun, “CD-MSA: Cooperative and Deadline-Aware Scheduling for Efficient Multi-Tenancy on DNN Accelerators,” IEEE Trans. Parallel Distrib. Syst., vol. 34, no. 7, pp. 2091–2106, Jul. 2023, doi: 10.1109/TPDS.2023.3276759.

[7] L. Lundberg, and H. Lennerstad. “Slack-based global multiprocessor scheduling of aperiodic tasks in parallel embedded real-time systems,” 2008 IEEE/ACS International Conference on Computer Systems and Applications, Apr. 2008.

[8] C. Jiang, G. Han, J. Lin, G. Jia, W. Shi, and J. Wan, “Characteristics of Co-Allocated Online Services and Batch Jobs in Internet Data Centers: A Case Study From Alibaba Cloud,” IEEE Access, vol. 7, pp. 22495–22508, 2019, doi: 10.1109/ACCESS.2019.2897898.

[9] Y. Zhang, Q. Guo, Y. Zhou, and H. Sun, “Frequency-constrained unit commitment for power systems with high renewable energy penetration,” International Journal of Electrical Power & Energy Systems, vol. 153, p. 109274, Nov. 2023, doi: 10.1016/j.ijepes.2023.109274.

979-8-3315-8138-1